# Análisis experimental de los parámetros de capa física en tecnología LTE utilizando módulo inalámbrico SIM7600G-H

## Experimental analysis of physical layer parameters in LTE technology using SIM7600G-H wireless module

J. E. Herrera-Rubio
DOI: https://doi.org/10.22517/23447214.26021
Scientific and technological research paper

**Abstract— The growth in demand for LTE network services has outpaced current technical requirements, making it necessary to conduct analyses and field studies to determine the use and performance of the radio spectrum. Measuring and detecting spectrum usage in LTE is fundamental for mobile operators seeking to optimize coverage and service. This paper presents a compact, modular LTE measurement platform integrating GPS-based geolocation for real-time acquisition and monitoring of key performance indicators (KPIs). The hardware architecture centers on an ESP32 microcontroller coupled with a SIM7600G-H LTE communication module, enabling the simultaneous capture of geographic coordinates, cell identifiers, and physical-layer power metrics. The portability of the measuring instrument, thanks to its battery power, facilitates data acquisition, providing autonomy for spectrum measurement activities. This offers a dynamic, efficient and low-cost solution for network fault diagnosis and mobile network planning. Using the experimental field methodology, it can be inferred that the SIM7600G-H module operates in a range between -32dBm and -59dBm with a good signal, and the mobile phone between -72dBm and -88dBm with a marginal signal with a tendency to disconnect at the edge of the cell. Finally, the advantages and uses of portable devices and their potential application in resizing mobile networks as a spectrum measuring tool are observed.**

***Index Terms*— cellular electromagnetic, mobile communication, propagation, radio propagation, wireless communication.**

***Resumen*— El crecimiento de la demanda del servicio en redes LTE ha superado los requerimientos técnicos actuales de ahí que es necesario realizar análisis y estudios de campo que permitan determinar el uso y el rendimiento del espectro radioeléctrico. La medición y detección del uso del espectro en LTE es fundamental para los operadores móviles que desean optimizar la cobertura y el servicio. Esta investigación utiliza un sistema modular compacto de tecnologías LTE con GPS para el seguimiento y monitoreo en tiempo real de los indicadores de servicio (KPI), integrando los datos en una placa con un microcontrolador ESP32 y un módulo de comunicación SIM7600G-H. Los datos obtenidos en tiempo real de la ubicación, identificador de celdas y niveles de potencia de los KPI se almacenan en una memoria micro SD para su filtrado, depuración y procesamiento.**

**La portabilidad del instrumento de medición facilita las capturas gracias a la alimentación por batería, lo que le da autonomía para actividades de medición del espectro. Con esto se ofrece una solución dinámica, eficiente y de bajo costo para el diagnóstico de fallas en la red y planificación de redes móviles; con la metodología experimental de campo se puede inferir que el módulo SIM7600G-H opera en un rango entre -32dBm a-59dBm con una señal buena y el móvil entre -72dBm a -88dBm con señal marginal con tendencia de desconexión en el borde de la celda. Finalmente se observan las ventajas y usos que tienen los equipos portátiles y su posible uso en el redimensionamiento de las redes móviles como instrumento para medir el espectro.**

***Palabras claves*— Celular, comunicación inalámbrica, comunicación móvil, propagación electromagnética propagación de radio**

This article was submitted for review on January 28, 2026. The funding was provided with the authors' own resources. The study was conducted to observe the behavior of an LTE module used for research within the GITENT research group, by researcher Jorge E. Herrera Rubio (jherrera@unipamplona.edu.co) at the University of Pamplona

## I. Introduction

THE spectrum planning process has been updated following ITU-R Recommendation [1], which promotes more efficient management using technical standards and specialized engineering equipment for spectrum measurement.

The main objective is to accurately identify and define coverage areas, thereby optimizing spectrum use [2]. Key performance indicators (KPIs) — including Reference Signal Received Power (RSRP), Received Signal Strength Indicator (RSSI), Reference Signal Received Quality (RSRQ), and Reference Signal-to-Noise Ratio (RSSNR) — are acquired through the SIM7600G-H module, as specified by the manufacturer Simcom [3], without reliance on third-party applications. These metrics are retrieved directly via AT commands over integrated network protocols, compatible with multiple operating systems. The radio signal characteristics of the physical layer between the UE and the eNodeB are governed by the specifications set forth in 3GPP TS 36.214. Measurements are additionally performed at upper protocol layers and serve as diagnostic indicators for assessing coverage extent and signal quality, among other parameters [4]. At the physical layer, the RSRP is calculated in the UE as the linear average power of the downlink reference (RS) signals across the channel bandwidth,

evaluated over the resource blocks (RB) that carry the specific RS associated with the service cell [5]. For intra-frequency measurements (where two cells share the same carrier frequency), the accuracy requirement is between ±2 and ±3 dB, while inter-frequency measurements reduce this tolerance to ±6dB. With approximation adjustments, expression (1) is applied to find the RSRP.

$$RSRP_{dBm} = RSSI_{dBm} - (10 * log_{10}(12 * BR)) \quad (1)$$

The RSRQ represents the relationship between the RSRP and the RSSI of the LTE carrier [6] and is obtained as follows (2):

$$RSRQ_{dB} = \left(10 * log_{10}(BR)\right) + RSRP_{dBm} - RSSI_{dBm} \quad (2)$$

The RSSI indicator determines the number of configured OFDM symbols and the measurement bandwidth over N number of BRs [6], of the UE from all sources, including active cells on the same channel. Finally, the advantages and uses of portable devices and their potential application in resizing mobile networks as a spectrum measuring tool are observed Therefore, the RSRQ value is relevant near the cell edge when signal quality must be maintained due to the strong dependence on the RSSP when a handover is made to the cell with better power [7], the RSSNR is calculated according to the previous standard with (3) [5]:

$$RSSNR_{dB} = RSSI_{dBm} - \left(10 * LOG_{10}(BR)\right) \quad (3)$$

The work presented in [8] demonstrated that the deployment of virtual instruments in a laboratory setting for radio engineering measurements can effectively substitute costly spectrum analysis equipment. From both experimental and predictive standpoints, cognitive radio (CR) systems employing hybrid learning algorithms have shown the capability to estimate parameters such as SNR, channel energy, and user state, achieving channel occupancy prediction accuracies of up to 96%, as reported in [9]. That study also addresses the simulation and empirical validation of CR devices, acknowledging certain limitations inherent to the observed dataset.

In [10], a comprehensive set of parameters — including received power, SNR, spectral occupancy, and fingerprint detection — was measured in the context of cooperative spectrum sensing using CR technology. This approach demands substantial real-time computational resources across a multiband spectrum. The methodology enables the identification of primary users, whose activity records are stored in a dedicated database, and the outcomes are benchmarked against classical digital signal processing techniques and neural network-based classifiers.

An alternative approach to multiband spectrum monitoring employs Software-Defined Radio (SDR) platforms, leveraging entropy-based techniques applied locally at the UE level to characterize power levels, bandwidth, and carrier frequency. The collected data is subsequently uploaded to a centralized database to construct radio environment maps, thereby enabling user localization within the network [10].

Through a systematic experimental review conducted across heterogeneous propagation environments [11], a structured methodology was developed to evaluate radio channel parameters and performance metrics, establishing a comparative framework between 4G and 5G technologies for the assessment of mobile broadband network performance.

## II. METHODOLOGY

Figure 1 shows how the methodology applied in the research works and describes the different phases and activities.

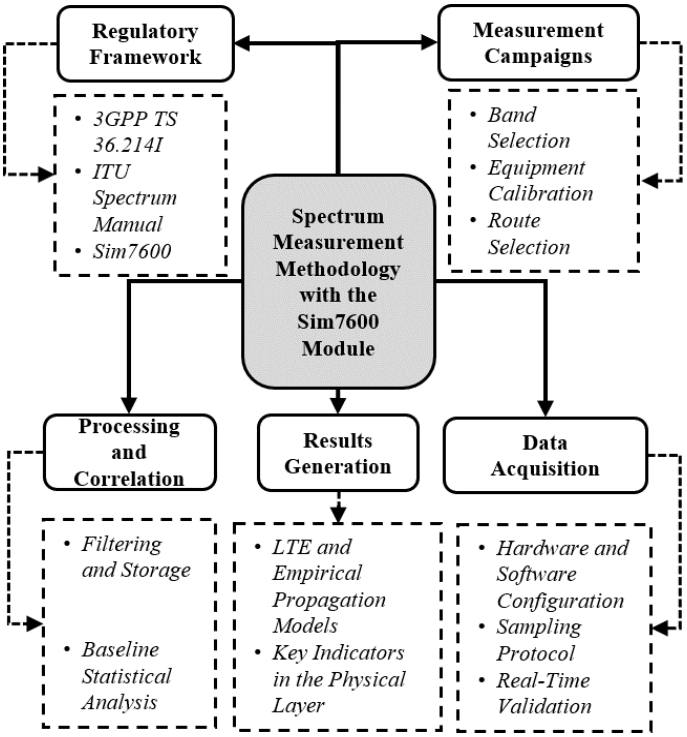


Fig. 1. Conceptual description of the methodology. Source: Authors.

### A. Regulatory Framework

3GPP TS 36.214: Version 3GPP TS 36.214 V17.0.0 defines the parameters present in measurements at the physical layer of the spectrum, including the ID, measurement type, commands (configure, modify, release), measurement objects, number of measurements, number of reports, and measurement criteria [6]. Standard establishes the minimum time- frequency unit for downlink transmission via BRs that are directly related to the RSSI. These BRs carry the reference signals to communicate with the UE when a physical channel is assigned at the physical layer [12].
ITU Technical Spectrum Verification Manual: This is used as a reference framework that integrates international guidelines and the analysis of factors influencing spectrum quality, such

as geographical conditions and site characteristics. It is based on the methodological principles defined by [13]. For measurement procedures and data evaluation, the practices established by [3]. are adopted, and the technical specifications and regulatory criteria are governed by the Radio Regulations of the [14].

Sim7600G-H: Using AT commands, this module offers an improved ability to collect important LTE network KPIs. It also provides useful information such as downlink (DL) and uplink (UL) frequencies, RF band, physical cell ID, service cell ID, and transmission bandwidth [15].

### A. Measurement Campaigns

Band Selection: Through scenario evaluation, frequency bands are identified where potential factors are identified as part of the study. These bands form the basis of the proposed scenario and are used to develop a forecast of the power to be measured at the nearest node [16].

Equipment calibration: This involves identifying sources of interference, even if the environment is not under control, addressing limitations of far-field interactions, ensuring sufficient height decoupling to avoid non-line-of-sight (NLOS) by minimizing potential obstructions, and preventing reflections and multipath effects [13].

Modern equipment typically includes a calibration source integrated into the measuring receivers and microprocessor-based analyzers for early detection of hardware errors, thus preventing erroneous data acquisition, as is the case with the SIM7600G-H [17].

Accuracy must account for systematic and stochastic errors resulting from the sweep speed and the electronic device's response when measuring power at short intervals; measurements can be continuous or repeated at regular intervals. Route Selection: This involves selecting four routes based on geographical orientations. Environmental parameters are adjusted, including band type, transmitter and receiver antenna height, power, gain, frequency, and initial receiver position [18]. All of this is done using the device, which continuously records data for short periods to study power level variations.

### B. Data Acquisition

Hardware and Software Configuration: The SIM7600G-H module was used, programmed via AT commands, with the following procedure: 1) Hardware configuration: Establish serial communication between the module and the Python microcontroller [19] using the TX and RX pins. Then, connect the LTE multiband antenna and insert a SIM card to detect the operator's network.

Next, observe the module's status LEDs to confirm that power and network registration are correct. 2) Visual Studio Code (VSC) IDE configuration: The Pymakr application, a VSC extension, is installed to facilitate the programming of MicroPython devices with the ESP32-WROVE-E [20] and the SIM7600G-H LTE chip. This allows communication with them via the Read Eval Print Loop (REPL). The files are then synchronized, the code is executed, and commands are sent directly to the module from the Python command editor [19]. 3) AT commands: In this step, calls are executed to obtain the physical layer frame field records between the SIM7600G-H module and the nearest eNodeBs, based on power detection and the test coverage area. 4) Code implementation: The code is executed, and the module is programmed as shown in Fig. 2 [21].

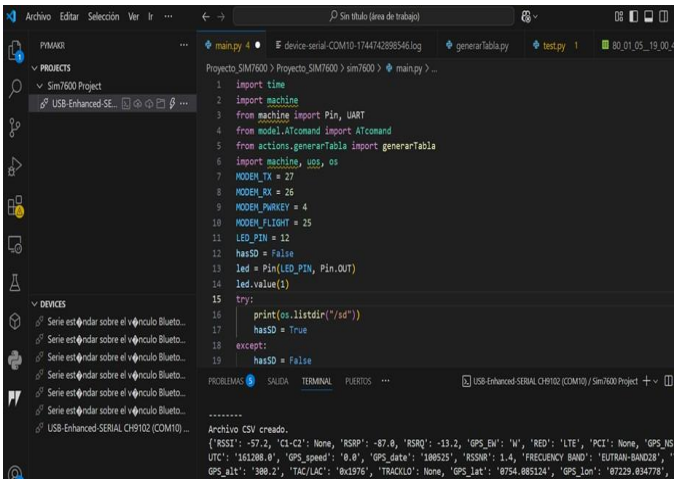


Fig. 2. Example of the SIM7600G-H module programming process.

Sampling protocol: Methodologically, spectrum measurement [22]with the test drive collects data on KPIs in specific areas, identifying the coverage of cells in service, interference, network changes, and coverage problems [23].

This indicates that, experimentally, measurements can be performed over short distances (between 10 m and 2 km) with low-cost modular equipment or smartphones that include GPS and software applications to predict power levels. For these spectrum measurement cases, the research in [7] proposes a guide to prediction methods to define the theoretical limits of interference and noise scenarios [10].

Based on this, propagation losses along a terrestrial path with direct or indirect line of sight must be considered, adding contributions such as: attenuation due to atmospheric gases, diffraction fading due to total or partial path obstruction as well as multiple paths, attenuation due to variations in the angle of arrival or launch, among others [24]. Real-time validation: This begins with configuring the system using the multiband antenna. The firmware is then configured with the capture protocol for sampling times in order to extract key parameters such as: cid, arfcn, band, rssi, rsrq, rsrp, system_time, Decimal_Latitude, and Decimal_Longitude [25] via AT commands. Changes in environmental conditions, data reporting latency, and the module's internal processing are also taken into account [26].

### C. Processing and Correlation

Filtering and Storage: The previously captured data was stored in the module within the micro-SD card in plain text

format. 180 samples were captured for each point on the different routes [8].

Simultaneously, the process was performed using the Netmonitor application on a mobile device for the same time, day, and geographical and atmospheric conditions. Erroneous or null data [27] were then filtered from the general database where the samples were stored for later analysis and interpretation.Outliers below this value (RSRP < -120 dBm) were eliminated [9]. Baseline Statistical Analysis: Each of the data points obtained from the samples was compiled into a file as a master database for all routes for the respective analysis, as shown in the capture example in Table I, in the section Annexes section.

Data processing, filtering, transformation, consolidation, and final reporting are achieved through coding with Python [28].The southern route is used as a reference to begin the analysis and coverage tests; the process is similar for the other routes. Initially, using the readings from the source files in Table 1, the RSSI value of the Honor UE (Fig. 3) is analyzed, which is the average power measured by the cell's BRs with respect to the channel bandwidth [8].

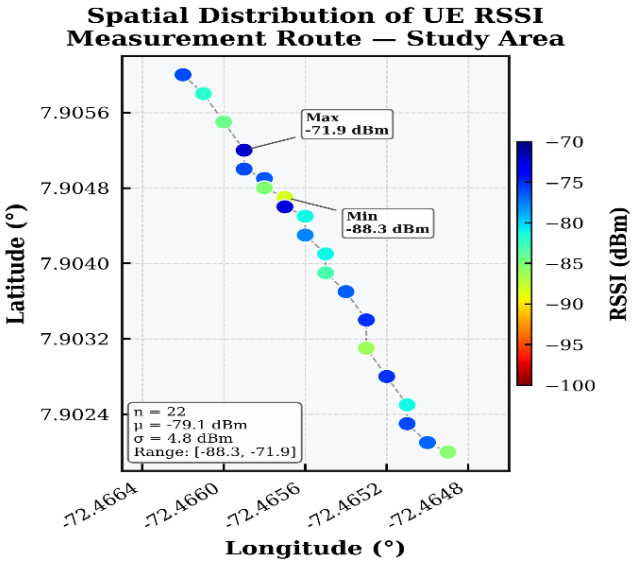


Fig. 3. RSSI samples taken with Honor mobile equipment. Source: Authors.

Figure 3 shows the RSSI intensity recorded by the UE along the measurement path, revealing a non-uniform signal distribution, with levels ranging from −71.9 dBm to −88.3 dBm (μ = −79.1 dBm, σ = 4.8 dBm). The strongest signals are predominantly observed near the base station. The moderate standard deviation (σ = 4.8 dBm) indicates a relatively stable RF environment with localized fading effects due to multipath propagation and partial obstruction along the path.

The levels reported by the EU are in the range of −100 to −116 dBm, with a mean of −106.9 dBm (σ = 4.8 dBm), indicating that most of the samples are in the poor category. In contrast, the SIM shows a significantly higher signal level, with a mean of −81.6 dBm (σ = 6.9 dBm), where 59% of the samples are in the good to excellent range.

There is a mean difference of Δ = 25.3 dBm between the two measurement methods, indicating systematic attenuation, possibly due to hardware losses and variability in propagation conditions (See Fig. 4).

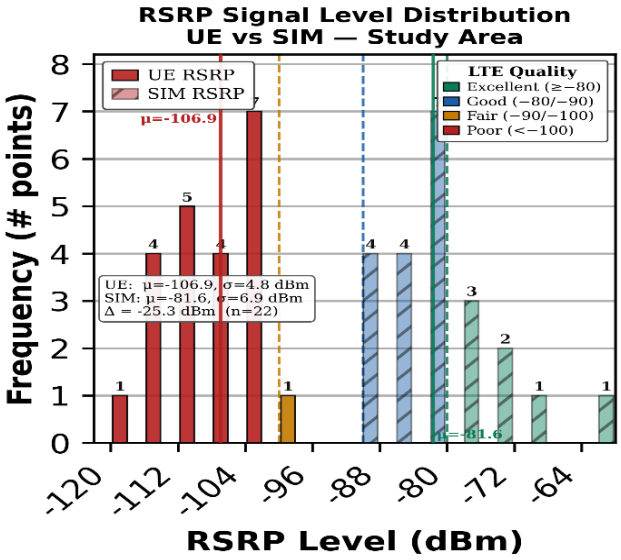


Fig. 4. Frequency histogram of RSRP signal levels measured across the study area. Source: Authors.

Similarly, when grouping the power levels (Fig. 5), the coverage areas of cells 311, 309, 267, and 125 are observed; cell 267 has the best coverage range along this route for the samples taken with the SIM7600G-H.

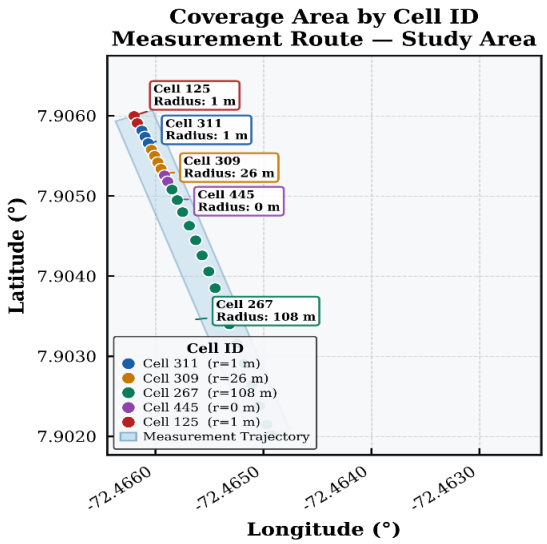


Fig. 5. RSRP samples with SIM7600G-H equipment for different CELL_IDs. Source: Authors.

The "Cell 445" could indicate that an antenna at the same measurement location generates a risk of interference; hardware delivery to Cell 309 at 12m could be causing potential saturation for nearby users due to the effect of multiple bands.

The KPIs are detailed below in general terms to define the behavior throughout the route, and an analysis by grouping the KPI values is performed as shown in Fig. 6.

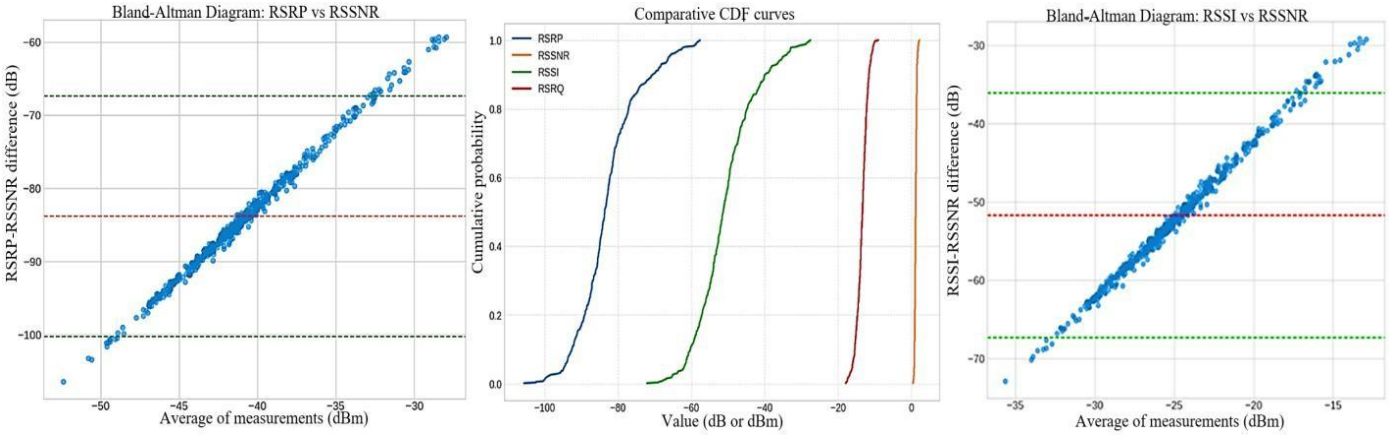


Fig. 6. KPI Analysis with SIM7600G-H Module. Source: Authors

On the left of Fig. 5, most samples cluster between -75 dB and -95 dB, indicating that the RSRP is generally lower than the RSSNR, but the cell locked to the UE maintains a very good average throughout the path. When the points disperse towards -90 dB to -100 dB, it indicates that when the RSRP is abnormally low compared to the RSSNR, problems arise due to: interference in the reference signal, hardware issues, or often, unusual propagation conditions [10].

In the center figure, with the Cumulative Distribution Function (CDF) [29], comparing the four metrics shows that: when the RSRQ is very close to zero, the signal quality is very high; Now, if the RSSNR diverges significantly, interference noise is present, possibly from other antennas (this occurs when 70% of the measurements are below 10 dB). When the RSRP

the left, there is no significant concentration of samples, as they are more dispersed around -105dB and -115dB of the RSRP. This is caused by unstable propagation due to cell handover and variable interference when selecting a better power from a neighboring cell. It may also be due to shadow fading and multipath effects.

In the central image, due to the data reading and filtering process, the RSRP shows regular coverage due to power drop. For the RSRQ, the signal quality is good, but with high variability. Regarding RSSI, the received power is relatively acceptable, but with interference, and coverage is maintained. In RSSNR, the signal is clean, and the SNR is consistent with low noise because the curve leans more towards positive values. There is slight variability (Fig. 6, right) between the total

diverges significantly, interference problems are likely (when it exceeds -110 dBm), and when the RSSI is high, noise contamination is possible (under optimal conditions, it is

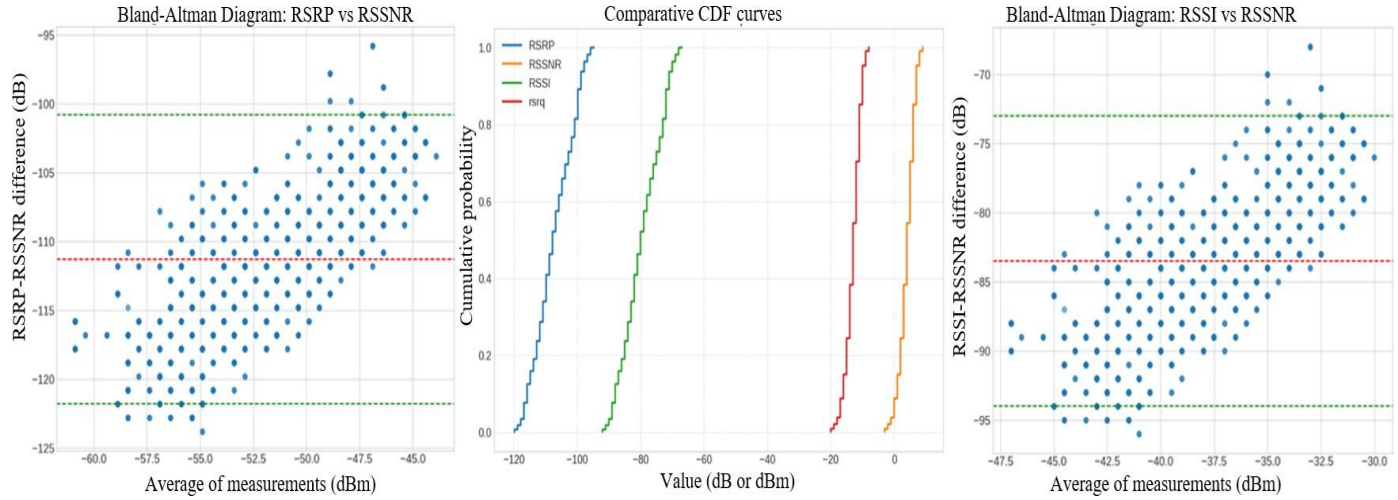


Fig. 7. KPI Analysis with Honor Mobile Device. Source: Authors

A difference in the capture format and mechanism is observed, possibly because the Honor device is connected to the LTE network with the services programmed by the operator. It is also using hardware resources that affect the wireless channel, making data digitization somewhat more complex, which explains the dispersion of the captured samples. In the image on

recommended to be between -60 dBm and -90 dBm).

Analyzing the figure on the right using the Bland-Altman plot [30], under normal operating conditions, a consistent RSSI-RSSNR difference and dispersion around the mean are obtained, with distribution patterns exhibiting minimal variability. However, in practice, extreme values are produced by the effect of adjacent cells due to channel reuse, as well as

by severe obstructions from moving objects such as vehicles and people [31].

In the case of measurements with the Honor mobile equipment, the assessments are similar in terms of the analysis as shown in Fig. 7 [32] with specific assessments in the measurements

RSSI power, ranging from -80 dBm to -90 dBm, but the signal is very good due to intercell interference [34]. RSSNR can also exhibit erroneous behavior at the receiver in response to external interference and the equipment hardware's ability to maintain a stable signal-to-noise ratio (SNR).

A. Generating Results

Propagation models for the LTE band: The models standardized by the ITU-R and 3GPP, applicable from 450 MHz to 6 GHz, are adapted to physical configurations in LTE networks [12].
Under line-of-sight (LOS) conditions, IMT- Advanced developed four 3D path loss models based on beams in the UE and urban environment scenarios: 3D macrocellular (UMa), microcellular (UMi), and outdoor-to-indoor UMa/UMi, for coverage between 10 m ≤ d ≤ dbreak; where dbreak is the distance to the maximum breakpoint where the signal is lost [33]. In UMi scenarios, the base station height is below the height of the surrounding rooftops, and in UMa scenarios, it is above the surrounding buildings.
For the proposed case study, (4) was used. This model assumes a base station height of 23 m and a microstation height of 1.5 m; where d is in meters and f is in GHz [34].

This model covers a maximum 3D modeling range of 2000 m

**The following variables and parameters are defined:**

**d**= distance in meters
**h** = average building height in meters
**h1** = UE height in meters
**ht** = base station height in meters
**f** = frequency in Megahertz
**hbreak** = cutoff height limit in meters
**ht** = base station height in meters
**hr** = UE height in meters
**W** = street width in meters
**fc** = central carrier frequency in Megahertz
**c** = constant defined by the COST-231 model
**a(hr)** = urban area height correction factor

$$PL_{3D\ UMI\ LOS}^{4G} = 40\log(d) + 28 + 20\log(f) - 9log[(h_{break})^2 + (h_t - h_r)^2] \quad (4)$$

The UMa LOS (3D LTE) equation before the breakpoint d ≤ d_break is represented by (5).

$$PL_{3D\ UMI\ LOS}^{4G} = 22\log(d) + 28 + 20\log(f) \quad (5)$$

When the breakpoint is d > d_break, the LTE standard recommends applying (4). If there is no line of sight (NLOS) in the same urban scenario, (6) is used.

$$PL_{3D\ UMI\ LOS}^{4G} = 36.7\log(d) + 22.7 + 26\log(f) - 0.3(h_r - 1.5) \quad (6)$$

If path loss occurs for 3D UMa NLOS, (7) is applied.

$$PL_{3D\ UMa\ NLOS}^{4G} = 161.04 - 7.1\log(W) + 7.5\log(h) - \left[24.37 - 3.7(\frac{h}{h_t})^2\right]\log(h_1) + [43.42 - 3.1\log(h_t)]\,[\log(d) - 3)] + 20\log(f) - \{3.2[\log(17.625)]^2] - 4.97\} - 0.6(h_t - 1.5) \quad (7)$$

The variable W represents the street width and h the average building height. The parameters involved in equation 7 are established as: 5 m < h < 50 m, 5 m < W < 50 m, 10 m < ht < 150 m, and 1.5 m < hr < 22.5 m.
For all LTE path loss models, shading is modeled as a zero-mean log-normal process, where its standard deviation ranges from 3 dB in UMi LOS, 4 dB in UMi NLOS and UMa LOS, 6 dB in UMa NLOS, to 7 dB in outdoor-to-indoor UMi/UMa environments [23].
Empirical propagation models: a) Okumura-Hata: uses (8) to determine losses in urban environments [33].

$$PL_{o-h} = 69.55 + 26.16\log(fc) - 3.82\log(ht) - a\log(hr) + (44.9 - 6.55\log(ht))\log(d) \quad (8)$$

The parameters fc are in MHz, ht (m) is the height of the transmitting antenna, d is the distance, and a (hr) is the correction factor for the receiving antenna. This factor is obtained using equation 9, and the frequency value is extrapolated if it exceeds the range of the expression.

$$a(hr) = (1.1\log(fc) - 0.7)hr - (1.56\log(fc) - 0.8);\ 150 \le fc \ll 1500 \quad (9)$$

b) The COST 231-Hata Model: This is a modification of the Okumura-Hata model [35], and the basic losses are calculated using (10), with c being a 3dB correction factor for urban environments [34].

$$PL_{c-231} = 46.3 + 33.9\log f - 13.82\log ht - 3.2(log(11.75hr))^2 - 4.97 + (44.9 - 6.55)\log d + c \quad (10)$$

A systematic analysis of the measured power evaluations and analytical representations yields the following trend curves in Fig. 8.

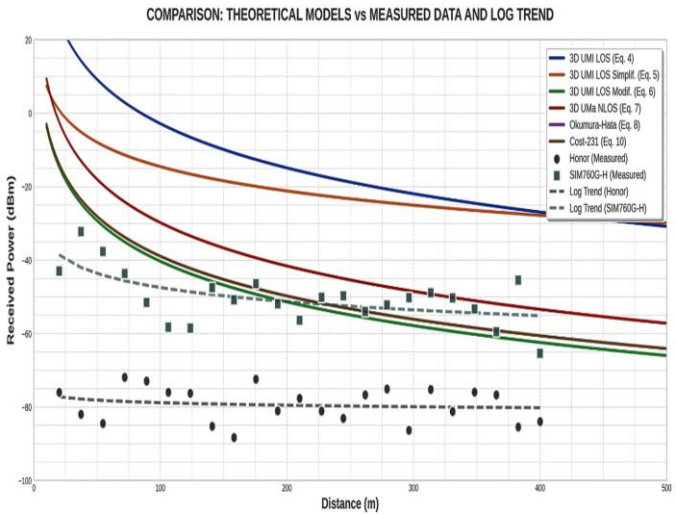


Fig. 8. Comparison of LTE models and field measurements. Source: Authors.

The comparative analysis between the trends of real devices and the theoretical models for LTE reveals significant discrepancies that are fundamental for the planning and validation of wireless networks. Both empirical trends exhibit an expected logarithmic decay of power with distance; the key difference lies in their vertical offset [36].

The UE Honor shows consistent superior receive power up to a distance of 100 meters. The measured power is noticeably higher than that of the SIM760G-H, indicating that the UE Honor, in this specific case, manages signal reception more effectively.

In the case of the SIM760G-H, although the path is parallel to that of the UE Honor, there is a considerable difference of several dBm below it. This constant phase shift indicates an additional system loss that is not due to the propagation channel, but rather to intrinsic factors of the device, such as antenna efficiency, receiver chipset sensitivity, or possibly firmware calibration. This means that the choice of terminal hardware is as critical a factor as cell coverage itself.

When comparing with theoretical LTE models, optimistic models like the 3D UMI LOS tend to overestimate the received signal strength because they assume ideal conditions (direct line of sight. no nearby obstacles) that are rarely fully met in a real-world environment. They do not quantify real-world factors such as diffraction in buildings, multipath propagation, or interference. In the Okumura-Hata model, designed for macrocellular environments, predictions are often more pessimistic and, in certain ranges, closer to the actual measurement. According to the graph, its curve more closely approximates the SIM760G-H's trend in the measurement range between 200 m and 400 m. This general trend exhibits logarithmic behavior, but the magnitude of the loss differs due to the complexities of the test environment, namely, the heterogeneity of the environment, the specific characteristics of the device, and the atmospheric conditions.

## III. DISCUSSION AND RESULTS

For the physical layer indicators, the RSRQ signal quality is typically between -3 dB and -10 dB under optimal conditions. Fig. 9 shows that the red line indicates where both devices report similar values, suggesting some correlation at each of the simultaneous measurement points.

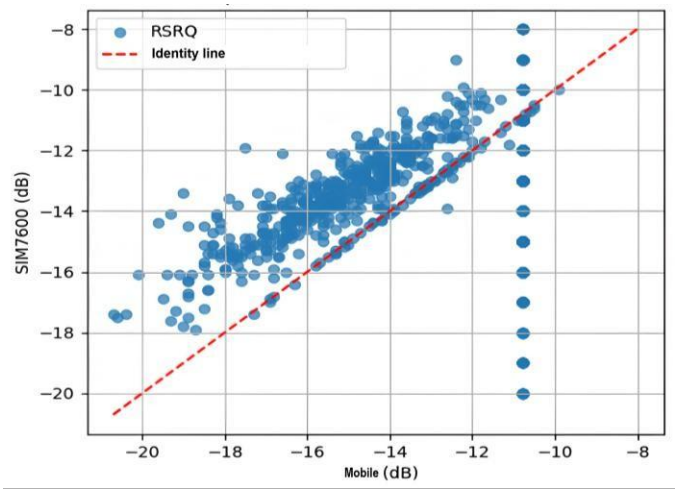


Fig. 9. Correlation of the RSRQ KPI between the two devices. Source: Authors

However, above the red line, the SIM7600G-H reports better quality than the mobile device; the highest concentration of RSRQ is between -12dB and -17dB. For the UE Honor, the values remain at the limit above the red line under acceptable measurement conditions. The vertical axis value between -10dB and -12dB is a measurement from the mobile device, which is an outlier and is not considered for the analysis, as it represents a momentary systematic error that scatters the data.

The possible differences can be limited to two scenarios: a) when the RSRQ values in the SIM7600G-H are higher than those of the mobile device, it exhibits better sensitivity in marginal areas with line of sight (LOS); b) in the case of lower values, there is a difference in the hardware and the measurement algorithm, which may be the result of an underestimation of signal quality.

In summary, the results of the measurements taken on a specific route, considering the KPIs and cell identifier (CID) presented in Table II, (in the section Annexes section) indicate that the RS-SINR measured at the user equipment (UE) at measurement points p3_m and p4_m shows a pronounced handover from cell 311 to cell 267. Subsequently, when the handover to cell 499 occurs, the power level remains stable throughout the entire analyzed route.

The UE's RSSI levels are lower, but this comes at the cost of RSRP quality, making it significantly lower due to noise and interference. The SIM7600G-H, lacking internal software optimizations, produces more realistic data for the radio environment, which may be suitable for propagation studies and spectrum characterization. However, the specifics of how the hardware discriminates between signal, interference, and noise are unknown.

For RSRQ, both devices maintain similar ranges of values, with the SIM7600G-H exhibiting lower dispersion and higher stability, suggesting greater accuracy in environments with highly fluctuating and dynamic changes. In terms of SINR, the Honor device is superior, likely due to its internal processing, which supports MIMO diversity and the device's DSP filters for reading data from LTE nodes.

The Honor showed a more favorable range between -90 dBm and -70 dBm for RSRP measurements, with better performance in normalization and power adjustments, while the SIM7600G-H registered values between -62 dBm and -100 dBm. The SIM7600G-H delivers unfiltered data, faithfully reproducing variations in the received signal, making it a precise tool for calibrations and coverage validations.

In the specific case of this analysis, a comparison of the values reveals significant differences between the two devices throughout the entire range, as seen in the RSSI (-25.84 dBm), RSRQ (0.534 Db), and RSRP (-24.741 dBm) for each measurement. These values represent the average differences between the two devices, indicating an inherent limitation in the measuring devices and their configuration, but not an error.

One possible reason is that the SIM7600G-H's antenna is slightly better because it focuses more energy effectively, is less susceptible to electromagnetic interference, and, in the case of mobile phone antennas, is compact and compromises gain and efficiency, which are reflected in the measurements. A graphical analysis details the KPIs during the route, see Fig. 10.

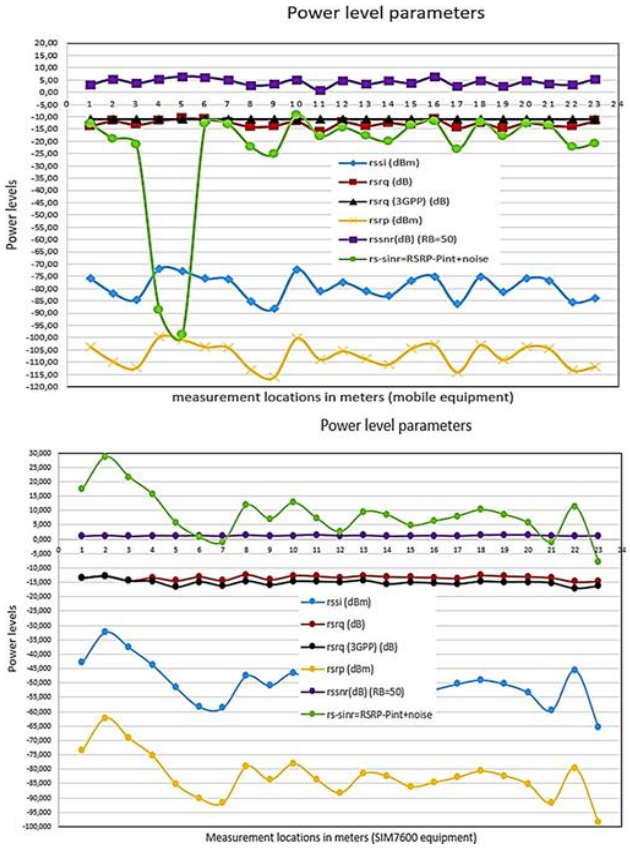


Fig. 10. Comparison of KPI results. Source: Authors

In the mobile equipment shown in the graph on the top, the RSSI variations between -70 dBm and -85 dBm indicate a relatively stable signal in most positions. The RSRP, ranging between -100 dBm and -115 dBm, is consistent with this type of technology, and the RSRQ and RSRQ 3GPP values are stable around -10 dB, indicating low interference. The RSSNR, with a value close to zero dB, shows slight variability, suggesting the presence of co-channel noise or thermal noise in the receiving equipment.

In the calculated RS-SINR, the variations are more pronounced, with very abrupt changes in the p3_m and p4_m measurements, indicating areas with high interference, either randomly and momentarily, or a loss of synchronization in the cell's wireless channel.

Finally, the graph on the bottom shows consistently higher RSSI levels (-60 dBm to -90 dBm) and RSRP values between -75 dBm and -95 dBm, indicating greater sensitivity in urban environments with high interference.

The RSRQ shows a uniform trend between -12 dB and -15 dB, with less dispersion, suggesting potentially more consistent measurements with less interference. Similarly, the RSSNR remains stable, indicating a realistic signal-to-noise ratio close to 5dB. The RS-SINR shows a trend toward positive values between 10 dB and 25 dB throughout the entire path, providing greater accuracy in the use of the signal relative to external interference.

Although the SIM7600G-H can be a connectivity and telemetry tool, it serves as an IoT cellular module in applied work, facilitating spectrum measurement, but it does not replace robust laboratory monitoring equipment.

## IV CONCLUSIONS

In practical terms, optimization of the analyzed KPIs in the mobile network is necessary, as the values they represent cause service quality problems during inter-cell connections. An acceptable correlation is evident in the central range of the measurements, with some differences at the extremes, especially near thresholds where service quality can worsen, as detailed in Figure 9. Similarly, the Bland-Altman tests quantify measurement biases by diagnosing the RSRP/RSSNR and RSSI/RSSNR. Therefore, calibration of both devices with a reference signal is required, as well as evaluating external effects during live testing. Furthermore, for mission-critical applications, SIM7600G-H modules and spectrum analyzers could be reliable for general monitoring of these parameters, but they do not replace laboratory equipment.

In cases where a site survey is conducted and network reports are generated indicating improved capacity with the use of the module, it is necessary to compare the results with a UE using a reliable application (e.g., Netmonitor) and more robust laboratory equipment. Therefore, a representation of the difference in measurements was achieved using a SIM7600G-H with a high-gain multiband antenna and a chipset optimized

specifically for real-time channel spectrum measurement, even at the same location.

A strong vertical dispersion is present in Figure 5 on the right (SIM7600G-H), indicating that the difference between RSRP and RSSNR will not be linear and depends on the channel and cell conditions. Therefore, the RSRP power level does not guarantee very good quality because inter-cell interference, thermal noise, and the cell's potential workload from serving other users come into play. In Figure 6b, the dispersion is higher and the difference is highly variable because the interference level fluctuates too much in nearby measurements. Thus, two users with the same RSSI can have very different link quality depending on interference from neighboring cells, and even more so with network congestion.

Finally, with limited data, machine learning and classification algorithms do not consider the physical characteristics of the working environment, which is why overfitting problems arise. However, they are a good reference point for analyzing large volumes of data. Theoretical models, on the other hand, are more practical since they consider more variables to analyze, but they are also subject to adjustments to improve their usability in mobile network planning. Looking ahead, for good initial planning, it is necessary to use better theoretical models combining Random Forest or K-Neighbors for fine-tuning and, where possible, validate them with independent measurements using more robust data.

The proposed modular and reconfigurable measurement architecture is a technical option as a basis for future adaptations aimed at low-power wide area network (LPWAN) technologies, particularly LTE-M and NB-IoT, which support the connectivity demands of Industry 4.0 ecosystems. The equipment used would allow for the systematic field characterization of IoT radio channels, such as coverage mapping, signal penetration in indoor and suburban environments, and the study of network load latency. This can be validated in NB-IoT and LTE-M measurement campaigns, with the aim of contributing to an open and reproducible instrumentation framework for research activities.

## REFERENCES

[1] M. U. Muzaffar y R. Sharqi, «A review of spectrum sensing in modern cognitive radio networks», *Telecommun. Syst.*, vol. 85, n.º 2, pp. 347-363, feb. 2024, doi: 10.1007/s11235-023-01079-1.

[2] M. Arawan, M. A. Bakri, y A. H. Paronda, «Optimasi Coverage Seluler Menggunakan Remote Electric Tilting Antena Sektoral E-Node B», 2022.

[3] SIMCom, «SIM7500_SIM7600 Series_ AT Command Manual LTE Module», n.º 289, 2021, [En línea]. Disponible en: www.simcom.com

[4] A. Al-Thaedan *et al.*, «Downlink throughput prediction using machine learning models on 4G-LTE networks», *Int. J. Inf. Technol. Singap.*, vol. 15, n.º 6, pp. 2987-2993, 2023, doi: 10.1007/s41870-023-01358-9.

[5] Z. Shakir, A. Y. Mjhool, A. Al-Thaedan, A. Al-Sabbagh, y R. Alsabah, «Key performance indicators analysis for 4 G-LTE cellular networks based on real measurements», *Int. J. Inf. Technol. Singap.*, vol. 15, n.º 3, pp. 1347-1355, 2023, doi: 10.1007/s41870-023-01210-0.

[6] 3GPP 3GPP TS 36.311, «Evolved Universal Terrestrial Radio Access (E-UTRA); Physical channels and modulation», vol. 2, 2025.

[7] P. P. G. 3GPP TS 34.121-1, «3GPP TS 34.121-1», *3rd Gener. Partnersh. Proj.*, vol. V16, 2019, [En línea]. Disponible en: https://www.3gpp.org/ftp/Specs/archive/34_series/34.121-1/

[8] S. Paramasivam y S. K. Nagarajan, «Cooperative spectrum sensing based hybrid machine learning technique for prediction of secondary user in cognitive radio networks», *J. Intell. Fuzzy Syst.*, vol. 44, n.º 3, pp. 3959-3971, 2023, doi: 10.3233/JIFS-222983.

[9] Y. Molina, A. Priete, R. Aguilar, y L. Miguel, «Cooperative Multiband Spectrum Sensing Using Radio Environment Maps and Neural Networks», *MDPI*, pp. 1-28, 2023.

[10] A. A. El-Saleh, M. A. Al Jahdhami, A. Alhammadi, Z. A. Shamsan, I. Shayea, y W. H. Hassan, «Measurements and Analyses of 4G/5G Mobile Broadband Networks: An Overview and a Case Study», *Wirel. Commun. Mob. Comput.*, vol. 2023, 2023, doi: 10.1155/2023/6205689.

[11] L. Zhang, S. Hu, M. Trik, S. Liang, y D. Li, «M2M communication performance for a noisy channel based on latency-aware source-based LTE network measurements», *Alex. Eng. J.*, vol. 99, pp. 47-63, jul. 2024, doi: 10.1016/j.aej.2024.04.063.

[12] Q. Zhu, C. Wang, B. Hua, K. Mao, S. Jiang, y M. Yao, *3GPP TR 38.901 Channel Model*, n.º January. 2021. doi: 10.1002/9781119471509.w5gref048.

[13] Union International Telecommunication, *Reglamento de Radiocomunicaciones*, 2024.ª ed., vol. 1. Suiza: UIT, 2024.

[14] I. Šimovček, L. Rajkovič, L. Gdovin, y J. Beňo, «Configuring IP Connectivity Over a Cellular Network on a Raspberry Pi - Based IoT Node», *Int. J. Inf. Technol. Appl.*, vol. 9, n.º 1, pp. 49-62, 2020.

[15] E. ETSI, «Harmonised european standar EN 301 908-18 V17.1.1», vol. 1, pp. 1-93, 2025.

[16] A. N. Abed, H. H. Waheed, B. A. Yousif, M. F. Ahmed, y T. A. Naji, «LTE Radio Resource Allocation according to ITU standard», 2023.
[17] D. E. Salhi, M. Rawashdeh, K.-D. Haouam, A. Alnusair, y A. Karime, «Smart Data Transmission in IoT: AI Applications for Health and Air Quality Monitoring», *Procedia Comput. Sci.*, vol. 272, pp. 294-302, 2025, doi: 10.1016/j.procs.2025.10.208.
[18] Asim. Zulfiqar, *HANDS-ON ESP32 WITH ARDUINO IDE unleash the power of IoT with ESP32 and build exciting projects with this practical guide*. 2024.
[19] M. Walker, «Python Data Cleaning Cookbook». Birminghan, Mumbai, 2021.
[20] J. Herrera, «Metodología de medición del espectro con técnicas experimentales para obtener modelos de propagación», vol. 1, p. 165, 2021.
[21] UIT-R, *Parámetros técnicos y de funcionamiento de los dispositivos de radiocomunicaciones de corto alcance y utilización del espectro por los mismos (Informe UIT-R SM.2153-8).*, vol. 8. Ginebra, Suiza, 2021. [En línea]. Disponible en: https://www.itu.int/pub/R-REP-SM.2153-8-2021
[22] ITU-R Recommendation P.1144-10, «Guide to the application of the propagation methods of Radiocommunication Study Group 3», vol. 10, n.º Geneva, Switzerland, 2019, [En línea]. Disponible en: https://www.itu.int/rec/R-REC-P.1144/en
[23] International Telecommunication Union (ITU): ITU-R Recommendation, *Propagation data and prediction methods for the planning of short-range outdoor radiocommunication systems and radio local area networks in the frequency range 300 MHz to 100 GHz P Series Radiowave propagation*, vol. P Series R. Geneva, Switzerland, 2019.
[24] T. S. ETSI TS 136 133, «ETSI TS 136 133 - LTE», *ETSI Evolved Univers. Terr. Radio Access*, vol. V16, 2020, [En línea]. Disponible en: https://portal.etsi.org/TB/ETSIDeliverableStatus.aspx
[25] N. Heydarishahreza y N. Ansari, «Mobile Node Localization in Wireless Networks: Path-Loss Model, Trilateration, and Error Mitigation in a 5G Sub-6 GHz Scenario», *J. Netw. Netw. Appl.*, vol. 3, n.º 3, pp. 129-136, 2023, doi: https://doi.org/10.33969/j-nana.2023.030304.
[26] N. Pilnenskiy y I. Smetannikov, «Feature selection algorithms as one of the python data analytical tools», *Future Internet*, vol. 12, n.º 3, 2020, doi: 10.3390/fi12030054.
[27] D. Ojuh y J. Isabona, «Empirical and Statistical Determination of Optimal Distribution Model for Radio Frequency Mobile Networks Using Realistic Weekly Block Call Rates Indicator», *Int. J. Math. Sci. Comput.*, vol. 7, n.º 3, pp. 12-23, 2021, doi: 10.5815/ijmsc.2021.03.02.
[28] P. Taffé, C. Zuppinger, G. M. Burger, y S. G. Nusslé, «The Bland-Altman method should not be used when one of the two measurement methods has negligible measurement errors», *PLOS ONE*, vol. 17, n.º 12, p. e0278915, dic. 2022, doi: 10.1371/journal.pone.0278915.
[29] G. K. Vishwakarma, C. Paul, y A. M. Elsawah, «An algorithm for outlier detection in a time series model using backpropagation neural network», *J. King Saud Univ. - Sci.*, vol. 32, n.º 8, pp. 3328-3336, 2020, doi: 10.1016/j.jksus.2020.09.018.
[30] K. M. Alari, S. B. Kim, y J. O. Wand, «A Tutorial of Bland Altman Analysis in A Bayesian Framework», *Meas. Phys. Educ. Exerc. Sci.*, vol. 25, n.º 2, pp. 137-148, 2021, doi: 10.1080/1091367X.2020.1853130.
[31] D. Dobrilovic, Z. Stojanov, J. Stojanov, y M. Malic, «Tools for modelling distance estimation based on RSSI», *CEUR Workshop Proc.*, vol. 2638, pp. 43-52, 2020, doi: 10.47350/iccs-de.2020.04.
[32] H. Tataria, K. Haneda, A. F. Molisch, M. Shafi, y F. Tufvesson, «Standardization of Propagation Models for Terrestrial Cellular Systems: A Historical Perspective», *Int. J. Wirel. Inf. Netw.*, vol. 28, n.º 1, pp. 20-44, 2021, doi: 10.1007/s10776-020-00500-9.
[33] I. M. M Mohamed, «Accurate Path-Loss Estimation for Wireless Cellular Networks», *J. Kejuruter.*, vol. 33, n.º 2, pp. 317-328, 2021, doi: 10.17576/jkukm-2021-33(2)-16.
[34] W. A. Ajibola y G. W. Ibrahim, «Journal of Engineering and Technology for Industrial Applications», *J. Eng. Technol. Ind. Appl.*, vol. 10, pp. 69-74, 2022.
[35] M. Bouzidi, M. Mohamed, Y. Dalveren, A. Moldsvor, F. A. Cheikh, y M. Derawi, «Propagation Measurements for IQRF Network in an Urban Environment», *Sensors*, vol. 22, n.º 18, pp. 1-21, 2022, doi: 10.3390/s22187012.
[36] T. Li, S. Hua, L. Kang, y S. H. Chang, «Research on TD-LTE wireless communication network propagation model optimization based on visual simulation and GIS», *Eurasip J. Wirel. Commun. Netw.*, vol. 2021, n.º 1, 2021, doi: 10.1186/s13638-021-02007-0.

# ANEXOS

TABLE I
DATA FORMAT RECORDED FOR EACH OF THE MEASUREMENTS. SOURCE: AUTHORS.

| **TIME** | RED | **ESTADO** | **MCC MNC** | **TAC_LAC** | **CELLID** | **FRECUENCY BAND** | **EARFCN_ARFCN** | **RSRQ (dB)** | **RSRP (dBm)** |
|---|---|---|---|---|---|---|---|---|---|
| 10 | LTE | Online | 732-103 | 0x1976 | 267 | EUTRA N-BAND4 | 2325 | -14,3 | -81,3 |
| 17 | LTE | Online | 732-103 | 0x1976 | 267 | EUTRA N-BAND4 | 2325 | -12,8 | -81,4 |
| 23 | LTE | Online | 732-103 | 0x1976 | 267 | EUTRA N-BAND4 | 2325 | -12,5 | -80 |

| **RSSI** (dBm) | **RSSNR** (dB) | **GPS_lat** | **GPS_lon** | **GPS_date** | **GPSUTC** | **GPS alt** | **Latitud Decimal** | **Longitud Decimal** | **SYSTM_TIME** |
|---|---|---|---|---|---|---|---|---|---|
| -48 | 0,8 | 754,16145 | 7229,14165 | 70625 | 194749 | 295,8 | 7,90269098 | -72,48 | 2007-06-25 19:47:49 |
| -50,3 | 1,3 | 754,16139 | 7229,14172 | 70625 | 194756 | 295,8 | 7,90268995 | -72,48 | 2007-06-25 19:47:56 |
| -48,8 | 0,5 | 754,16139 | 7229,14175 | 70625 | 194802 | 295,8 | 7,90268998 | -72,48 | 2007-06-25 19:48:02 |

TABLE II

COMPARISON OF KPIS BETWEEN THE TWO DEVICES. SOURCE: AUTHORS.

| **Physical layer parameters for Honor mobile device** | | | | | | | | **Physical layer parameters for SIM7600G-H device** | | | | | | | |
|---|---|---|---|---|---|---|---|---|---|---|---|---|---|---|---|
| Reference point | rssi (dBm) | rsrq (dB) | rsrq (3GPP) (dB) | rsrp (dBm) | rssnr (dB) (RB=50) | rs-sinr | cid | Reference point | rssi (dBm) | rsrq (dB) | rsrq (3GPP) (dB) | rsrp (dBm) | rssnr(dB) (RB=50) | rs-sinr | cid |
| p0_m | -75,96 | -13,89 | -10,79 | -103,7 | 3,1 | -12,93 | 445 | p0_s | -42,95 | -13,56 | -13,52 | -73,46 | 1,03 | 17,35 | 311 |
| p1_m | -82 | -11,75 | -10,79 | -109,8 | 5,24 | -18,97 | 309 | p1_s | -32,26 | -12,89 | -12,89 | -62,14 | 1,24 | 28,67 | 309 |
| p2_m | -84,5 | -13,32 | -10,79 | -112,3 | 3,67 | -21,47 | 124 | p2_s | -37,66 | -14,43 | -14,5 | -69,15 | 0,97 | 21,66 | 309 |
| p3_m | -71,91 | -11,62 | -10,79 | -99,69 | 5,37 | -88,79 | 311 | p3_s | -43,68 | -13,4 | -14,6 | -75,27 | 1,19 | 15,54 | 267 |
| p4_m | -72,93 | -10,63 | -10,79 | -100,7 | 6,36 | -99,01 | 311 | p4_s | -51,56 | -14,42 | -16,61 | -85,16 | 1,11 | 5,65 | 267 |
| p5_m | -75,97 | -10,91 | -10,79 | -103,8 | 6,08 | -12,94 | 267 | p5_s | -58,33 | -13,13 | -14,82 | -90,14 | 1,21 | 0,67 | 267 |
| p6_m | -76,23 | -12,15 | -10,79 | -104 | 4,84 | -13,2 | 499 | p6_s | -58,58 | -14,35 | -16,16 | -91,73 | 1,04 | -0,92 | 267 |
| p7_m | -85,27 | -14,15 | -10,79 | -113,1 | 2,83 | -22,24 | 499 | p7_s | -47,5 | -12,36 | -14,54 | -79,03 | 1,32 | 11,78 | 267 |
| p8_m | -88,29 | -13,81 | -10,79 | -116,1 | 3,18 | -25,27 | 499 | p8_s | -50,86 | -14,07 | -15,89 | -83,74 | 1,09 | 7,07 | 267 |
| p9_m | -72,39 | -11,95 | -10,79 | -100,2 | 5,04 | -9,36 | 499 | p9_s | -46,42 | -12,68 | -14,66 | -78,08 | 1,25 | 12,73 | 267 |
| p10_m | -81,03 | -16,16 | -10,79 | -108,8 | 0,83 | -18 | 499 | p10_s | -51,9 | -12,89 | -14,7 | -83,58 | 1,41 | 7,23 | 267 |
| p11_m | -77,63 | -12,24 | -10,79 | -105,4 | 4,75 | -14,6 | 499 | p11_s | -56,4 | -13,28 | -14,85 | -88,24 | 1,15 | 2,57 | 267 |
| p12_m | -81,09 | -13,78 | -10,79 | -108,7 | 3,21 | -17,9 | 499 | p12_s | -50,1 | -12,69 | -14,32 | -81,42 | 1,26 | 9,39 | 267 |
| p13_m | -83,07 | -12,45 | -10,79 | -110,9 | 4,54 | -20,05 | 499 | p13_s | -49,75 | -13,05 | -15,61 | -82,35 | 1,01 | 8,46 | 267 |
| p14_m | -76,66 | -13,31 | -10,79 | -104,4 | 3,68 | -13,63 | 499 | p14_s | -54,03 | -13,23 | -14,99 | -86,01 | 1,1 | 4,8 | 267 |
| p15_m | -75,11 | -10,89 | -10,79 | -102,9 | 6,1 | -12,08 | 499 | p15_s | -52,26 | -13,35 | -15,29 | -84,54 | 1,2 | 6,27 | 267 |
| p16_m | -86,31 | -14,64 | -10,79 | -114,1 | 2,35 | -23,28 | 499 | p16_s | -50,25 | -13,6 | -15,56 | -82,8 | 1,06 | 8,01 | 267 |
| p17_m | -75,22 | -12,5 | -10,79 | -103 | 4,49 | -12,19 | 499 | p17_s | -48,91 | -12,64 | -14,68 | -80,57 | 1,34 | 10,24 | 267 |
| p18_m | -81,25 | -14,78 | -10,79 | -109 | 2,21 | -18,23 | 499 | p18_s | -50,34 | -12,89 | -14,91 | -82,25 | 1,36 | 8,56 | 267 |
| p19_m | -75,93 | -12,49 | -10,79 | -103,7 | 4,5 | -12,9 | 499 | p19_s | -53,33 | -13,05 | -14,85 | -85,17 | 1,37 | 5,64 | 267 |
| p20_m | -76,68 | -13,6 | -10,79 | -104,5 | 3,39 | -13,65 | 499 | p20_s | -59,54 | -13,45 | -15,18 | -91,72 | 1,16 | -0,91 | 267 |
| p21_m | -85,43 | -13,9 | -10,79 | -113,2 | 3,09 | -22,4 | 499 | p21_s | -45,45 | -14,81 | -17,05 | -79,49 | 1,07 | 11,32 | 125 |